

Research on the Measurement System and Remote Calibration Technology of a Dual Linear Array Camera

Bin Feng^{1*}, Zaiming Liu¹, Haofei Zhang², Haozhe Fan¹

¹*School of Optoelectronic Engineering, Xi'an Technological University, Xi'an 710021, China, fengbin@xatu.edu.cn*

²*No.208 Research Institute of China Ordnance Industries, Beijing 102202, China*

Abstract: In order to accurately measure the flight trajectory of the projectile in a long-distance target range, it is important to establish a vertical target measurement system with a two-line array camera at several positions along the range. In the present work, a calibration system using dual theodolites is proposed to calibrate the vertical target measurement system of a dual linear array camera at different positions along a long target range. The present study investigates the principle of intersection measurement in the vertical target measurement system with a double linear array camera and presents the projectile's target coordinate measurement formula. The calibration method of the measurement system is developed based on an analysis of the parameters in the projectile coordinate measurement formula. The calibration method only requires calibration of the camera's distortion coefficient, the optical axis angle, and the principal point, ensuring a simplified and expedited calibration process. After calibration, the vertical target measurement system with a $3\text{ m} \times 3\text{ m}$ measurement area is simulated and analyzed, yielding an error distribution diagram and identifying the factors that influence the measurement accuracy of the projectile's target coordinates.

Keywords: Dual linear array camera, vertical target measuring system, impact coordinates, long-distance target range, error analysis.

1. INTRODUCTION

In order to acquire the flight trajectory of projectiles in the extensive spatial domain of a long-distance target range, it is imperative to establish several target measurement systems for the output of impact point coordinate information, long-distance is the distance range defined as 1~300 m with reliable measurement accuracy of the theodolite used. The trajectory of the projectile is then reconstructed based on the impact point coordinate information derived from each individual target measurement system.

Current methods for impact point coordinate measurement include optoelectronic fusion [1], [2], [3], multi-screen intersection measurement [4], single-line array Charge-Couple Device (CCD) target measurement [5], acoustic principles, laser target measurement [6] and binocular intersection measurement [7], [8], [9]. Within the extended spatial limits of a long-distance target range, the acquisition of high-precision impact point coordinate information is of utmost importance for the representation of the projectile's flight trajectory. To achieve a higher degree of consistency in the output coordinates from multiple target measurement systems within the expansive spatial domain of a long-distance target range, dual-line array CCD intersection measurement offers significant advantages. Dual-line array

CCD intersection measurement is a commonly used non-contact measurement technique that is characterized by its simple measurement principles, ease of engineering integration, high measurement accuracy and capacity for measuring multiple targets.

However, the traditional dual-line array CCD target measurement is not suitable for precision measurements on large target surfaces. The test target surface of the equipment is relatively small, and installation and debugging are challenging. Existing models for dual-line array camera intersection measurements assume a fixed triangle formed by two cameras and the impact point, which requires precise measurement of the pitch angles of the two cameras and the distance between them. The coordinates (x, y) of the impact point are then determined by solving the triangle. In this study, a new model for the coordinate measurement of the point of impact is derived by investigating the structural design of a dual-line array camera target measurement system suitable for intersection measurements on a large target surface of $3\text{ m} \times 3\text{ m}$. The new mathematical model does not require prior measurement of the camera pitch angles or the distance between the cameras. When cameras are used for measurement, it is important to determine the true geometric position of the projectile and the corresponding point in the

image. The geometric model of camera imaging is used to describe this correspondence, and the parameters of the geometric model are solved by associating known world coordinates of feature points with pixel coordinates. Horaud et al. [10] proposed a two-step method for line scan camera calibration based on the cross-ratio invariance. Subsequent research by Li et al. [11] considered the influence of first-order radial distortion of the lens. Traditional methods for calibrating line-scan cameras involve calibrating both the internal and external parameters of the camera [4], [12], [13], [14], which is a complex and labor-intensive process. In this study, a dual theodolite measurement system is used to calibrate two cameras. The dual theodolite measurement system provides the world coordinates of feature points [15] and the cameras output the pixel coordinates corresponding to these feature points. The relationship between the pixel coordinates and the feature point offsets is then solved. This method does not require repeated calibration, and both the calibration process and the calculation are simplified. Moreover, compared with the close-range calibration of other projectile coordinate measurement systems [16], [17], the dual-linear array camera measurement system and the remote calibration method can enlarge the measurement screen surface from $0.5\text{ m} \times 0.5\text{ m}$, $1\text{ m} \times 1\text{ m}$ to $3\text{ m} \times 3\text{ m}$, while ensuring high-precision measurement of projectile coordinates.

2. VERTICAL TARGET MEASUREMENT SYSTEM BASED ON A DUAL-LINE ARRAY CAMERA

The schematic diagram in Fig. 1 illustrates the composition principle of the vertical target measurement system using a dual linear array camera.

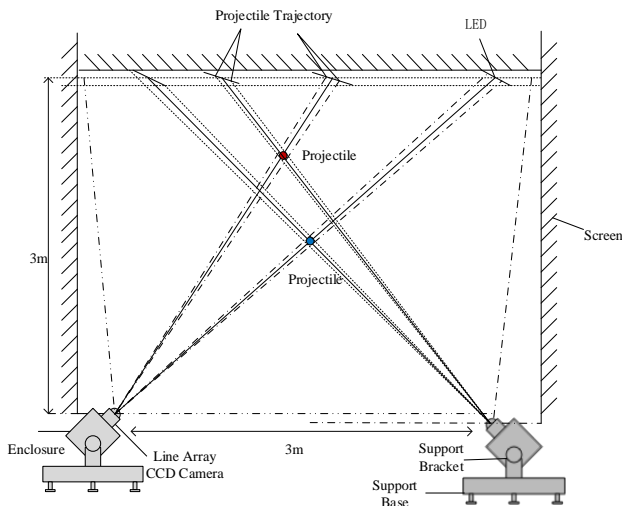


Fig. 1. Schematic diagram of dual-line array CCD camera collimation measurement system.

The vertical target measurement system consists primarily of two linear array cameras, a Light Emitting Diode (LED) surface light source and a supporting structure. The supporting structure consists of a casing, a reinforcing frame and a stabilizing foundation. The LED surface light source is attached to the side and top of the dual linear array cameras.

The viewing angle of the optical system lens for the linear array camera is more than 90° , so that the detection fields of the dual linear array cameras are aligned in one plane, forming a measurement screen surface of about $3\text{ m} \times 3\text{ m}$. The projectile target is simultaneously captured by two linear array cameras as it passes through the measurement screen, and the digital image information of the projectile target is output separately. The computer system processes the acquired image of the projectile target and extracts the position coordinates of the projectile target on the sensor of the online array camera. Finally, the x and y coordinates of the projectile on the measurement screen are calculated using the formula for the projectile's target coordinates.

The schematic diagram in Fig. 2 illustrates the calculation principle used to determine the target coordinates of the projectile.

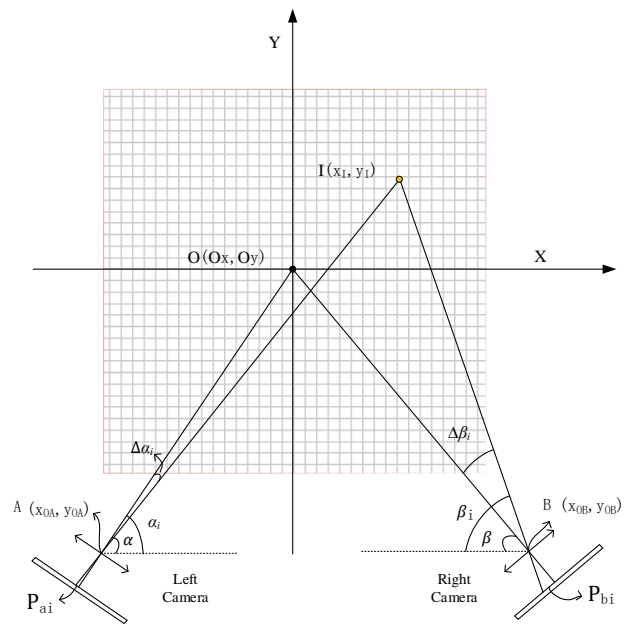


Fig. 2. Schematic diagram of system impact point coordinate calculation.

The coordinate system is defined by taking the intersection point $O(O_x, O_y)$ of the optical axis of the optical system of the two linear array cameras as the coordinate origin, i.e. the intersection point of the line OA and the line OB . Assume that $A(x_{OA}, y_{OA})$ is the main point of the left linear array camera optical system and $B(x_{OB}, y_{OB})$ is the main point of the right camera optical system, where α is the inclination of the left camera's optical axis and β is the inclination of the right camera. The pixel coordinates of point I on the left and right camera sensors are denoted as P_{ai} and P_{bi} , respectively, by the image processing.

The inclination angles corresponding to point I are α_i and β_i , respectively, while the offsets from the inclination angles of the two optical axes are $\Delta\alpha_i$ and $\Delta\beta_i$. From the geometric relationship between the lines shown in Fig. 2, it can be deduced that the point of intersection between line AI and line BI represents the coordinates of the impact.

$$\begin{cases} y_I - y_{OA} = (x_I - x_{OA}) \tan(\alpha - \alpha_i) \\ y_I - y_{OB} = (x_I - x_{OB}) \tan(\beta - \beta_i) \end{cases} \quad (1)$$

$$x_I = \frac{y_{OB} - y_{OA} - x_{OB} \tan \Delta \beta_i}{\tan \Delta \alpha_i - \tan \Delta \beta_i} \quad (2)$$

$$y_I = y_{OB} + (x_I - x_{OB}) \tan \Delta \beta_i \quad (3)$$

In the above equation:

$$\Delta \alpha_i = \alpha - \alpha_i \quad (4)$$

$$\Delta \beta_i = \beta - \beta_i \quad (5)$$

Equations (1)-(5) show that to determine the coordinates of the point of impact, it is necessary to calibrate the optical center coordinates of the left camera lens and the right camera lens, the inclination of the optical axis of the two cameras, and the functional relationship between $\Delta \alpha_i$ and $\Delta \beta_i$ and P_{ai} and P_{bi} .

3. CALIBRATION OF VERTICAL TARGET MEASUREMENT SYSTEM IN LONG-DISTANCE TARGET RANGE

A. Calibration method

Calibration of the vertical target measurement system comprises two contents:

1. establishing the distortion model of the optical system and finding the corresponding relationship between the parameters of each camera;
2. specifying the position coordinates of the main point of the camera and the optical axis inclination of the optical system of the two cameras.

We consider the camera imaging system as a "black box system". As long as the relationship between the pixel coordinates of the target on the camera sensor and the angular offset of the optical center line between the target and the lens is obtained, the lens distortion coefficient can be solved and the calibration of the imaging system can be completed.

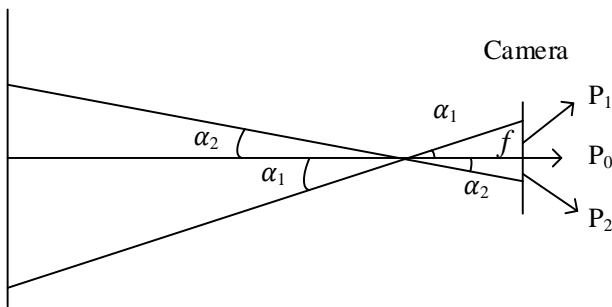


Fig. 3. Camera imaging diagram.

Fig. 3 is the imaging diagram of the camera. Let the focal length of the camera be f . It results from the triangular geometric relationship:

$$\alpha_i = \arctan\left(\frac{P_i}{f}\right) \quad (6)$$

In the vertical target coordinate measurement system with a measurement area of $3 \text{ m} \times 3 \text{ m}$, the lens distortion of the

linear array camera has a significant effect on the measurement results of the impact point coordinates. The presence of lens distortion leads to a certain deviation between the image element P_i captured by the camera sensor and its ideal counterpart \hat{P}_i , resulting in significant errors in the accurate calculation of the coordinates of impact. We apply the calibration method to correct the lens distortion. This involves creating a mathematical model that relates the actual pixel coordinates to the ideal pixel coordinates of the target.

The lens distortion primarily comprises:

- the radial distortion $\delta_r = k_1 x(x^2 + y^2)$,
- the tangential distortion $\delta_d = p_1 x(3x^2 + y^2) + 2p_2 xy$,
- the thin prism distortion $\delta_p = s_1(x^2 + y^2)$ and
- the tilt distortion $\delta_l = a_0 x + a_1 y + a_2 xy + a_3$.

The assembly of the optical lens in the linear array camera usually has a minimum deviation, thus higher-order distortions beyond three orders are generally disregarded. Consequently, the lens distortion model can be expressed succinctly as follows:

$$P_i = k_1 \hat{P}_i^3 + k_2 \hat{P}_i^2 + k_3 \hat{P}_i + k_4 \quad (7)$$

In (7), $k_i (i = 1, \dots, 4)$ is the distortion coefficient. To reduce the calculation difficulty, let $\alpha_i' = \tan(\alpha_i)$, $k_i' = k_i/f$, and thus the lens distortion model can be expressed as:

$$\alpha_i' = k_1' \hat{P}_i^3 + k_2' \hat{P}_i^2 + k_3' \hat{P}_i + k_4' \quad (8)$$

Equation (8) shows that the offset of the target relative to the optical axis has a certain functional relationship with the pixel coordinates and the equation does not include the focal length of the lens and the baseline distance between the two cameras. Therefore, the measurement system for the opposite target only needs to be calibrated once, and it is not necessary to repeatedly calibrate the opposite target measurement system after changing the lens and adjusting the baseline distance of the two cameras. Therefore, this calibration method is suitable for the calibration of the vertical target measurement distributed at different positions in the long-distance target path, the calibration process is simple and fast and the calculation is small. It is also possible to calibrate the angle of the optical axis of the camera optical system and the position of the main point of the lens in each vertical target measurement system using the double theodolite.

B. Calibration process

An analog rod mounted on the calibration bracket is used to represent the projectile passing through the measuring screen and the end face of the analog rod is provided with crosshairs that can be used for theodolite long-range aiming. A double theodolite measuring system is used to measure the analog rod at different positions on the surface of the measuring screen. The two-dimensional coordinates of the analog rod on the surface of the measuring screen are specified, thus establishing the mathematical plane equation of the measuring screen surface, as shown in Fig. 4.

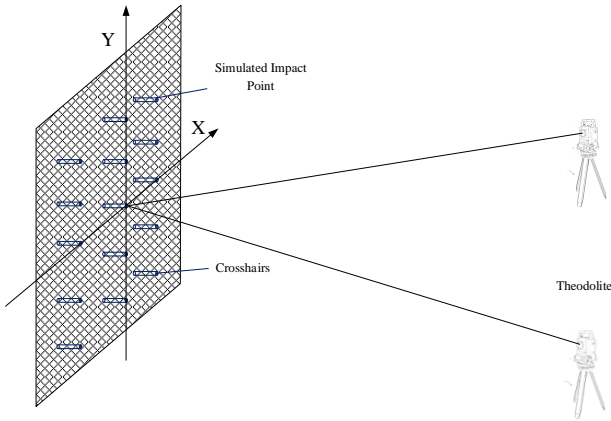


Fig. 4. Schematic diagram of the calibration process.

After the two theodolites are accurately aligned, a standard ruler of known length is measured to calculate the base length of the two theodolites using the spatial solution equation.

The angle of the optical axis and the coordinates of the main point of the dual linear array camera lens are first determined. By processing the acquired analog rod image, the pixel coordinate value on the camera sensor is obtained, and then a functional relationship can be established according to the angle offset of the optical axis relative to the connection between the analog rod and the lens optics, which clearly reflects the pixel coordinate and the angle offset. Through this function, the analog rod coordinate can be measured on the entire measurement screen.

4. ERROR ANALYSIS AND SIMULATION OF VERTICAL TARGET MEASUREMENT SYSTEM

The impact coordinate measurement equations (2) and (3) show that x_I and y_I can be regarded as functions of the independent variables x_{OB} , y_{OB} , x_{OA} , y_{OA} , $\Delta\alpha_i$, $\Delta\beta_i$.

If these independent variables are differentiated separately, the error transfer coefficient is obtained: dx/dn , dy/dn , where $n = \Delta\alpha_i$, $\Delta\beta_i$, x_{OB} , y_{OB} , x_{OA} , y_{OA} . According to the error transfer theory, the standard deviation of the measurement error of coordinates and coordinates is:

$$\sigma_x^2 = \left(\frac{\partial x}{\partial \Delta\alpha_i}\right)^2 \Delta(\Delta\alpha_i)^2 + \left(\frac{\partial x}{\partial \Delta\beta_i}\right)^2 \Delta(\Delta\beta_i)^2 + \left(\frac{\partial x}{\partial y_{OA}}\right)^2 \Delta y_{OA}^2 + \left(\frac{\partial x}{\partial y_{OB}}\right)^2 \Delta y_{OB}^2 + \left(\frac{\partial x}{\partial x_{OB}}\right)^2 \Delta x_{OB}^2 \quad (9)$$

$$\sigma_y^2 = \sigma_x^2 + \left(\frac{\partial x}{\partial \Delta\beta_i}\right)^2 \Delta(\Delta\beta_i)^2 + \left(\frac{\partial x}{\partial y_{OB}}\right)^2 \Delta y_{OB}^2 + \left(\frac{\partial x}{\partial x_{OB}}\right)^2 \Delta x_{OB}^2 \quad (10)$$

According to (9) and (10), the coordinate measurement error is related to the position of the optical center of the camera lens and the deviation angle of the line on which the target point is located relative to the optical axis. The control variable method is used to simulate the standard deviation of the coordinate measurement error caused by a certain parameter within a certain range, with the aim of investigating the individual influence of each parameter on the measurement results.

It is assumed that there is no error between the calibrated pixel coordinates and the corresponding angle offset, i.e. $\Delta(\Delta\alpha_i) = 0$, $\Delta(\Delta\beta_i) = 0$. From (2) and (3), it can be seen that the target coordinates (x_I, y_I) of the projectile are independent of the x-coordinate values of the optical center position of the left camera lens.

Let the y-coordinate of the optical center position of the left camera lens be $y_{OA} = -1019.85$ mm and the optical center position coordinates of the right camera lens be $x_I = 1405.86$ mm, $y_I = 1053.59$ mm. According to (9) and (10), it can be seen that σ_x and σ_y increase with the increase of the absolute values of the right camera optical center coordinates x_{OB} and y_{OB} and the error has a linear relationship.

Due to the high measurement accuracy of the theodolite, the position offset of the optical center of the camera lens is also small, so the direction of the main point of the camera lens on the right side is equal to the direction offset distance, i.e. $\Delta x_{OB} = \Delta y_{OB}$.

Fig. 5 shows the corresponding variations of σ_x and σ_y when the impact point coordinates are $x_I = 1405.86$ mm and $y_I = 1053.59$ mm, under the condition: $|x_{OB}| = |y_{OB}| \leq 3.5$ mm.

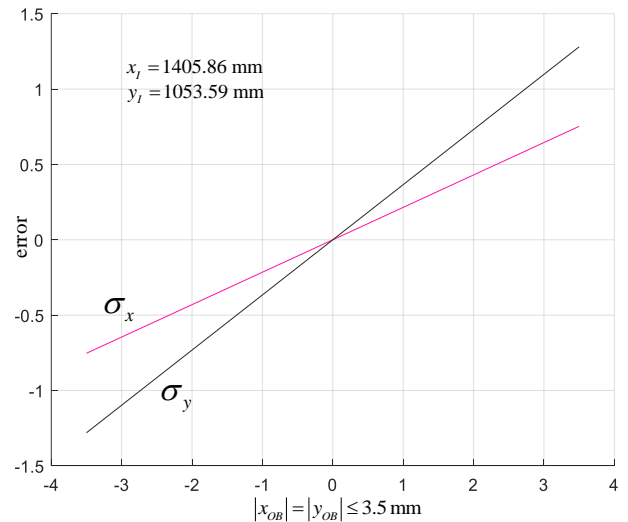


Fig. 5. Trend of measurement error with right camera lens light center position.

Similarly, if the other parameters remain unchanged, the y-coordinate of the optical center of the left camera lens is shifted and σ_x and σ_y increase with the increase of the y-coordinate position $|y_{OA}|$ of the optical center of the left camera lens. When $|y_{OA}| \leq 3.5$ mm, the corresponding changes are shown in Fig. 6.

Assume that the position of the optical center of the left and right camera lens is determined and equal to $(x_{OA}, y_{OA}) = (186.69$ mm, -1019.85 mm) and $(x_{OB}, y_{OB}) = (2592.02$ mm, -1010.54 mm), respectively. If the optical system of the left camera is calibrated, we obtain $\Delta(\Delta\alpha_i) = 0$, $\Delta(\Delta\beta_i) = 1^\circ$. The entire measurement screen is simulated under this condition. The lens used has an angle of 90° . Within the range of $|\Delta\alpha_i| = |\Delta\beta_i| \leq 45^\circ$, the variation trend of the measurement error is shown in Fig. 7.

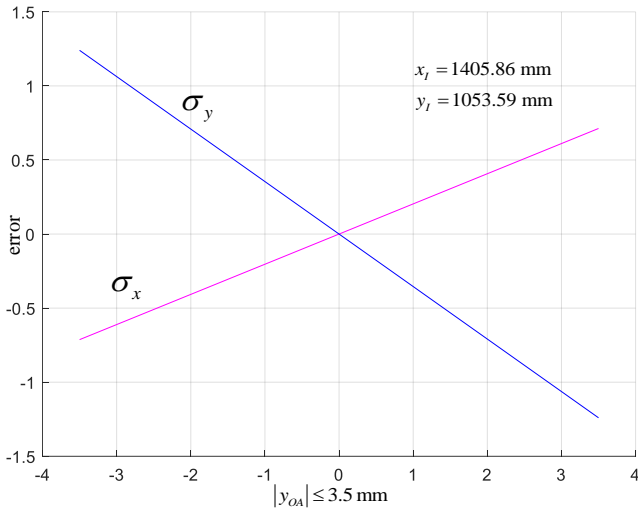
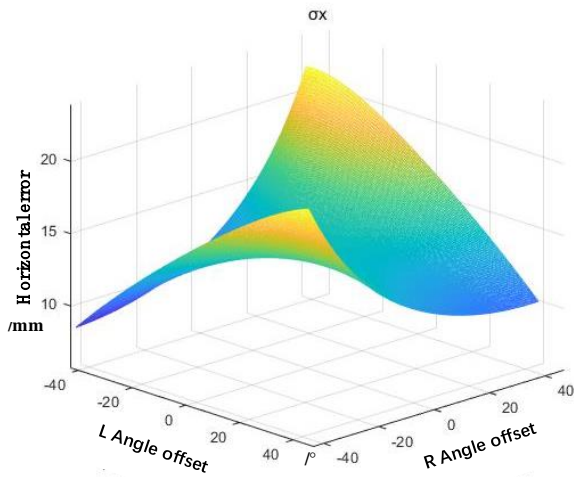
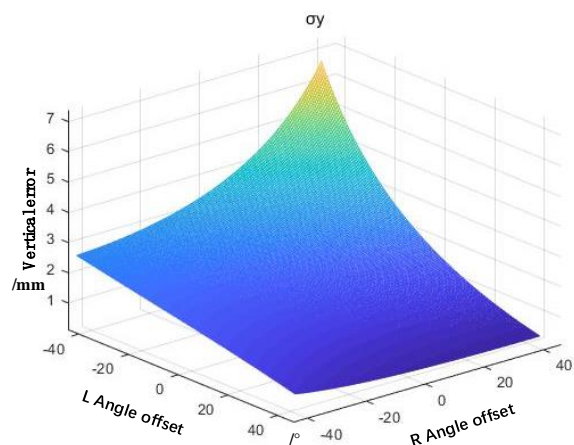


Fig. 6. Trend of measurement error with left camera lens light center position.

Similarly, if $\Delta(\Delta\beta_i) = 0$ and $\Delta(\Delta\alpha_i) = 1^\circ$, the other parameters remain unchanged and σ_x and σ_y fulfill the condition $|\Delta\alpha_i| = |\Delta\beta_i| \leq 45^\circ$, the variation trend of the measurement error is shown in Fig. 8.



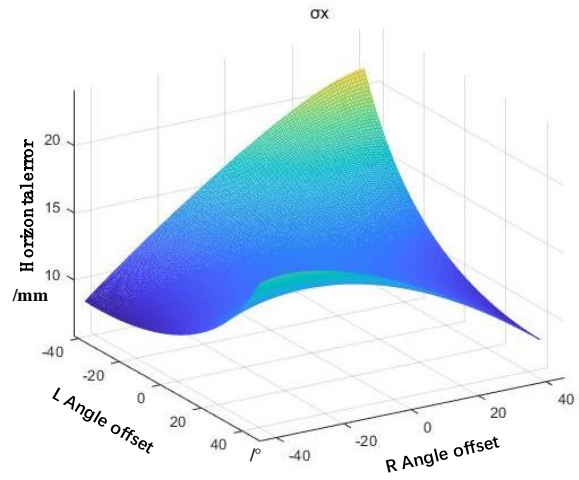
(a)



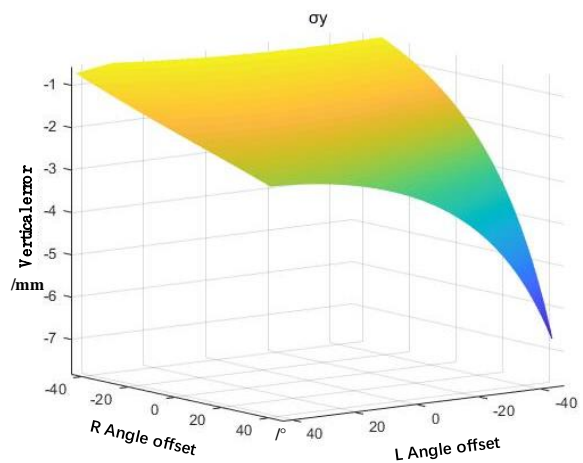
(b)

Fig. 7. The trend of measurement error with $|\Delta\alpha_i|$ and $|\Delta\beta_i|$ ($\Delta(\Delta\beta_i) = 1^\circ$).

From Fig. 7 we can obtain $8 \text{ mm} \leq \sigma_x \leq 27 \text{ mm}$, $0.5 \text{ mm} \leq \sigma_y \leq 7 \text{ mm}$.



(a)



(b)

Fig. 8. The trend of measurement error with $|\Delta\alpha_i|$ and $|\Delta\beta_i|$ ($\Delta(\Delta\alpha_i) = 1^\circ$).

From Fig. 8, we can obtain $8 \text{ mm} \leq \sigma_x \leq 25 \text{ mm}$, $-8 \text{ mm} \leq \sigma_y \leq -0.5 \text{ mm}$.

Fig. 7 and Fig. 8 show that the error term generated by the angle offset of the lens has a major influence on the measurement error of the impact point coordinates.

Due to the high accuracy of the theodolite measurement system, the error of the main point of the lens can be ignored. Since the image of the projectile target through the optical system is more than 5 pixels, the center of the image of the projectile can be accurately determined using the centroid solving algorithm. Under the above conditions, let $\Delta(\Delta\alpha_i) = \Delta(\Delta\beta_i) = 0.003 \text{ rad}$. The measurement screen is simulated again and the variation trend of the angle offset and of σ_x and σ_y is determined. The simulation results are shown in Fig. 9.

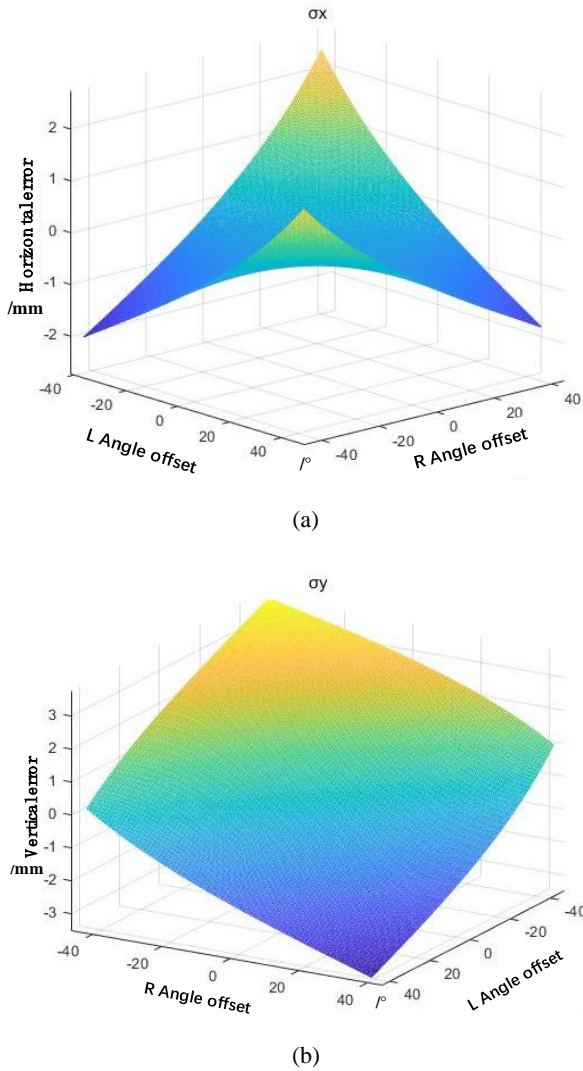


Fig. 9. The trend of measurement error with $|\Delta \alpha_i|$ and $|\Delta \beta_i|$ ($\Delta (\Delta \alpha_i) = \Delta (\Delta \beta_i) = 0.003$ rad).

5. SYSTEM ACCURACY VERIFICATION EXPERIMENT

Table 1 shows the coordinate data of the impact points measured by the system. Due to the $3\text{ m} \times 3\text{ m}$ measurement surface, the experiment was divided into two groups to achieve accurate precision in measuring the surface. The experimental setup included two sets of experiments with the central coordinates of the intersection point of the two optical axes, x and y , of (1438.72 mm, 189.59 mm). For the central region, one set of experiments provided the data shown in Table 1, and another set of experiments was performed for the edge region and provided the data shown in Table 2. In Table 1 and Table 2, PL and PR represent the pixel center coordinates output from the left and right cameras, respectively. The reference values x_0 and y_0 correspond to the coordinates measured with the dual theodolite measurement system, while x_I and y_I represent the coordinates of the impact points measured with the collimation measurement system.

The experimental data in Table 1 show that the measurement error of the x-direction coordinates for the impact points in the central region ranges from a minimum of -1.31 mm to a maximum of 1.41 mm. For the y-direction coordinates, the measurement error ranges from a minimum of -3.08 mm to a maximum of 1.70 mm. Further calculations show that the standard error in the x-direction is 0.75 mm for the central region and 1.14 mm for the y-direction.

The experimental data in Table 2 show that the measurement error of the x-direction coordinates for the impact points in the edge region ranges from a minimum of -3.70 mm to a maximum of 2.81 mm. For the y-direction coordinates, the measurement error ranges from a minimum of -2.79 mm to a maximum of 2.73 mm. Further calculations show that the standard error in the x-direction is 2.68 mm for the edge region and 2.27 mm for the y-direction.

Table 1. Experimental data from the central area of the collimation measurement surface.

NO.	Standard values [mm]		Pixel coordinates [px]		Impact point coordinates [mm]		Measurement error [mm]	
	x_0	y_0	PL	PR	x_I	y_I	Δx	Δy
1	634.32	-326.86	-336	-719	634.85	-326.37	0.52	0.48
2	644.24	488.42	-781	-220	645.08	485.34	0.83	-3.08
3	934.75	861.42	-640	59	936.16	859.66	1.41	-1.76
4	930.17	490.09	-514	-104	930.44	489.04	0.26	-1.04
5	927.27	88.52	-312	-327	927.76	87.66	0.48	-0.86
6	1134.80	863.40	-500	152	1135.33	862.21	0.52	-1.18
7	1130.43	492.28	-359	-9	1131.25	491.75	0.82	-0.53
8	1127.70	90.33	-143	-236	1128.04	89.27	0.34	-1.05
9	1125.15	-323.24	193	-551	1126.21	-323.32	1.06	-0.07
10	1120.06	-782.87	814	-1053	1118.75	-782.47	-1.31	0.39
11	1466.50	867.33	-304	332	1465.24	869.03	-1.25	1.70
12	1461.87	495.98	-150	178	1461.66	496.94	-0.20	0.96
13	1458.87	94.20	73	-48	1458.54	94.32	-0.33	0.11
14	1456.20	-319.40	395	-383	1455.87	-319.77	-0.32	-0.36
15	1450.91	-779.04	925	-962	1451.04	-778.60	0.12	0.44

Table 2. Experimental data for the edge region of the target measurement surface.

NO.	Standard values [mm]		Pixel coordinates [px]		Impact point coordinates [mm]		Measurement error [mm]	
	x_0	y_0	PL	PR	x_I	y_I	Δx	Δy
1	2468.14	-968.32	1260	-720	2466.07	-966.60	-2.06	1.71
2	2419.21	-945.26	1240	-700	2417.78	-947.43	-1.42	-2.17
3	416.99	1273.21	-1146	6	419.10	1270.72	2.11	-2.48
4	623.73	1196.36	-965	52	620.38	1194.88	-3.34	-1.47
5	803.84	1212.76	-825	130	806.32	1215.47	2.48	2.71
6	256.15	-957.96	-6	-1330	252.87	-955.22	-3.27	2.73
7	320.31	-736.69	-522	-1123	323.12	-739.47	2.81	-2.78
8	423.65	-527.77	-523	-926	426.19	-526.86	2.54	0.90
9	327.64	-838.78	-231	-1212	324.40	-836.43	-3.23	2.34
10	2471.94	1287.82	-31	1182	2468.23	1285.16	-3.70	-2.65

6. CONCLUSION

The present study investigates the measurement principle of a vertical target measurement system using a double linear array camera. It derives the measurement formula for determining the impact point coordinates and analyzes the error associated with this measurement system. This paper presents a unified calibration method for multiple vertical target measurement systems in a long-distance target range using dual theodolites. The calibration method provides three parameters: the distortion coefficient, the angle of the optical axis, and the camera's principal point. Finally, a mapping relationship is established between the pixel coordinates of the target and its deviation angle relative to the linear array camera's optical axis. Numerical simulations of the vertical target measurement system have shown that any position error in the main point of the optical lens can lead to a linear error in the vertical target measurement system. In addition, an inaccurate mapping between the target pixel coordinates and the offset angles can significantly affect the measurement accuracy of the vertical target measurement system. Compared with the close-range calibration of other projectile coordinate measurement systems, the double-linear array camera measurement system and the remote calibration method can increase the measurement screen surface from $0.5 \text{ m} \times 0.5 \text{ m}$, $1 \text{ m} \times 1 \text{ m}$ to $3 \text{ m} \times 3 \text{ m}$, while ensuring high-precision measurement of projectile coordinates. The live firing test of the vertical target measuring system with a $3 \text{ m} \times 3 \text{ m}$ measurement screen is finally carried out. The experimental results show that the measurement system has an absolute error of less than 3.8 mm in the x-direction and less than 3.0 mm in the y-direction, which is in excellent agreement with the numerical simulation results.

ACKNOWLEDGMENT

This research was funded by the Shaanxi Science and Technology Department (Program No.2020GY-158), and the 2022 "Insight Action" Achievement Transformation and Application Project (Program No. 628020320).

REFERENCES

- [1] Lu, S.-T., Chou, C., Lee, M.-C., Wu, Y.-P. (1993). Electro-optical target system for position and speed measurement. *IEE Proceedings A*, 140 (4), 252-256.
- [2] Li, H., Lei, Z. (2013). Projectile two-dimensional coordinate measurement method based on optical fiber coding fire and its coordinate distribution probability. *Measurement Science Review*, 13 (1), 34-38.
- [3] Chang, C. C., Chang, H. C., Tang, L. C., Young, W. K., Wang, J. C., Huang, K. L. (2005). Hybrid-integrated prism array optoelectronic targeting system. *Optics & Laser Technology*, 37 (8), 591-596. <https://doi.org/10.1016/j.optlastec.2004.11.002>
- [4] Xia, R., Hu, M., Zhao, J., Chen, S., Chen, Y. (2018). Global calibration of multi-cameras with non-overlapping fields of view based on photogrammetry and reconfigurable target. *Measurement Science and Technology*, 29 (6), 65005. <http://dx.doi.org/10.1088/1361-6501/aab028>
- [5] Dong, T., Hua, D., Li, Y., Ni, J. (2014). Measuring principle of vertical target density based on single linear array CCD camera. *Optik*, 125 (1), 176-178. <https://doi.org/10.1016/j.ijleo.2013.07.006>
- [6] Li, H., Zhang, X., Miao, W. (2019). Spatial position measurement of multiple targets using a line lasers and a plane array camera. *IEEE Sensors Journal*, 19 (22), 10443-10451. <https://doi.org/10.1109/JSEN.2019.2931802>
- [7] Zhu, L., Yang, X., Xu, C., Xu, T., Jiang, L. (2020). Analysis on the motion characteristics of dynamic aircraft by dual-line-array TDI CCD optical camera. *Optoelectronics Letters*, 16 (1), 1-6. <https://doi.org/10.1007/s11801-020-9015-3>
- [8] Lv, J., Shi, P., Wan, Z., Cheng, J., Xing, K., Wang, M., Gou, H. (2022). Research on a real-time monitoring method for the three-dimensional straightness of a scraper conveyor based on binocular vision. *Mathematics*, 10 (19), 3545. <https://doi.org/10.3390/math10193545>
- [9] Lei, M., Zhang, X., Dong, Z., Wan, J., Zhang, C., Zhang, G. (2023). Locating anchor drilling holes based on binocular vision in coal mine roadways. *Mathematics*, 11 (20), 4365. <https://doi.org/10.3390/math11204365>
- [10] Horaud, R., Mohr, R., Lorecki, B. (1993). On single-scanline camera calibration. *IEEE Transactions on Robotics and Automation*, 9 (1), 71-75. <https://doi.org/10.1109/70.210796>

- [11] Li, D., Wen, G., Wei Hui, B., Qiu, S., Wang, W. (2014). Cross-ratio invariant based line scan camera geometric calibration with static linear data. *Optics and Lasers in Engineering*, 62, 119-125.
<https://doi.org/10.1016/j.optlaseng.2014.03.004>
- [12] Ma, W., Dong, T., Tian, H., Ni, J. (2014). Line-scan CCD camera calibration in 2D coordinate measurement. *Optik*, 125 (17), 4795-4798.
<https://doi.org/10.1016/j.ijleo.2014.04.057>
- [13] Huo, J., Zhang, G., Cui, J., Yang, M. (2018). Corrected calibration algorithm with a fixed constraint relationship and an error compensation technique for a binocular vision measurement system. *Applied Optics*, 57 (19), 5492-5504.
<http://dx.doi.org/10.1364/AO.57.005492>
- [14] Wu, J., Liu, G. (2012). Noniterative calibration of a camera lens with radial distortion. *Measurement Science and Technology*, 23 (10), 105013.
<http://dx.doi.org/10.1088/0957-0233/23/10/105013>
- [15] Fu, Q., Zhao, F., Zhu, R., Liu, Z., Li, Y. (2023). Research on the intersection angle measurement and positioning accuracy of a photoelectric theodolite. *Frontiers in Physics*, 10.
<https://doi.org/10.3389/fphy.2022.1121050>
- [16] Dong, T., Gao, F., Chen, D., Yang, J. (2020). Recognition method of the dual-objective in a linear array CCD-based improved photoelectric measurement system using two lasers with different wavelengths. *Optik*, 217, 164857.
<https://doi.org/10.1016/j.ijleo.2020.164857>
- [17] Wu, Z., Ma, J., Zhang, X., Ni, J. (2018). Research on accurate calibration method of screen plane equation of sky screen vertical target. *Optik*, 174, 86-90.
<https://doi.org/10.1016/j.ijleo.2018.08.051>

Received November 28, 2023

Accepted April 29, 2024